Impurity-defect interaction in ion-implanted supersaturated Au-Fe alloys

A. Turos* and O. Meyer
Kernforschungszentrum Karlsruhe, Institut für Nukleare Festkörperphysik, Postfach 3640, D-7500 Karlsruhe, Federal Republic of Germany
(Received 26 November 1984)

The annealing behavior of Au-implanted Fe single crystals has been studied by means of the channeling and backscattering technique. Room-temperature implants of $(3-5)\times 10^{16}$ Au ions/cm^2 at 700 keV resulted in metastable supersaturated Au-Fe alloys. Large changes of the Au depth distributions and the lattice-site location were found after isothermal anneal sequences. Three well-distinguished annealing stages were observed: stage 1, 350—450 °C—precipitation of Au; stage 2, 500—650 °C—migration of Au towards the surface; and stage 3, over 650 °C—back-diffusion of Au into the bulk. The analysis of the time dependence of these processes leads to the conclusions that migration of vacancy-impurity complexes with an activation energy $E_a=1$ eV is the dominant mechanism in stages 1 and 2, whereas in stage 3 the solubility-limited diffusion with $E_a=2.9$ eV takes place.

I. INTRODUCTION

During the past few years a number of experimental and theoretical investigations have been directed toward a basic understanding of ion-implanted supersaturated alloys and their annealing behavior.[1–4] Increased atomic mobilities in solids during irradiation due to the flow of radiation-produced point defects are well known as radiation-enhanced diffusion or radiation-induced segregation.[5] However, if the implantation temperature is below the migration stage of vacancies, stage III, similar defect-impurity interactions and enhanced migration may be observed during thermal annealing at temperatures above stage III but well below temperatures where normal bulk diffusion is observed. The point-defect migration stages for Fe are briefly summarized in Sec. IV.

Annealing of irradiated metals usually produces a broad spectrum of recovery stages. This is due to the production of several defect species during irradiation and their interactions upon annealing. The flow of point defects to sinks such as dislocations, voids, and external surfaces can induce segregation of impurities at the sinks via defect-assisted migration. Complications of this simple picture arise from defect-cluster formation and agglomeration. With increasing annealing temperature the clusters decay, thus providing a large number of free point defects. These temperature-dependent nonequilibrium phenomena affect the diffusional and segregational behavior of impurity atoms and thus influence all basic kinetic processes and material properties. When finally the temperature of an implanted system is sufficiently high for all of its constituents to be mobile, the phases are formed following the equilibrium phase diagrams.

One objective of this work was to study the thermal kinetics for the solute segregation and diffusion of a metal-in-metal implant where the solubility limit is greatly exceeded. Such a condition is frequently present in high-dose implantations performed for the modification of surface properties. A second objective was to measure the solid solubility of Au in bcc iron as a function of temperature. Finally, our research also has been stimulated by the study of the corrosion behavior of Au-implanted Fe.[6] The preliminary results of the study of thermal stability of ion-implanted Fe have been published elsewhere.[7]

II. EXPERIMENTAL DETAILS

Single-crystal slices of high-purity iron were cut with the [110], [100], and [111] axes approximately normal to the surface. They were lapped and then electropolished until the resultant surfaces had a mirrorlike appearance. Prior to implantation all crystals were analyzed using a 2-MeV ^{4}He-ion-channeling technique.[8] The energy resolution of the detection system was 14 keV, which provides a depth resolution of about 20 nm for depths up to about 500 nm. Minimum yield values of 3—5 % have been obtained. Implantation of 700-keV Au ions was carried out at room temperature. During implantation the crystals were tilted by 10° with respect to the low-index crystal directions to avoid channeling effects. The beam-current densities used were less than 1 μA/cm^2 and the fluence was $(3-5)\times 10^{16}$ Au ions/cm^2. After implantation the specimens were annealed in a vacuum furnace at 10^{-6} Torr and at temperatures ranging from 350 to 900 °C.

III. RESULTS

A. As-implanted case

Figure 1 shows the random and ⟨110⟩-aligned spectra for a Au-implanted Fe single crystal. Helium ions backscattered from Au atoms are well separated in energy from those backscattered from Fe atoms. Therefore lattice-location and depth profiles of the impurities can be easily studied. The large reduction of both host- and impurity-scattering yields in the aligned case indicates that (a) the Fe crystal has suffered only moderate lattice

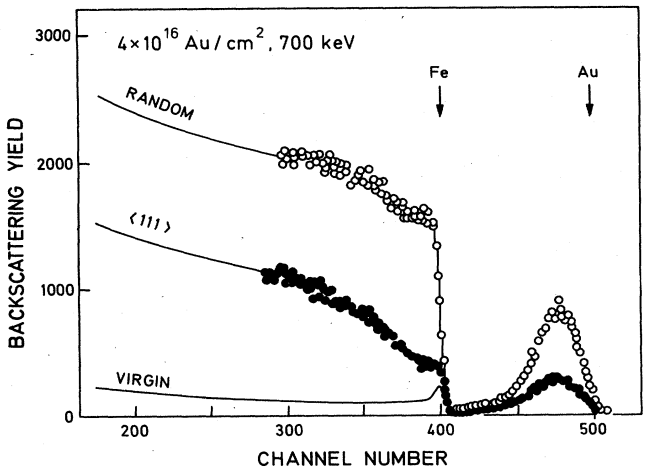

FIG. 1. Random and aligned backscattering spectra for 2-MeV ^{4}He ions from a Au-implanted Fe single crystal.

damage by Au implantation, and (b) the Au atoms are highly substitutional.

The depth of the maximum in the Au distribution, corresponding to a concentration of 7 at. %, is 70 nm. The implanted Au extends deeply into the host crystal. The experimentally estimated variance and skewness of the Au distribution are much higher than calculated from the Lindhard-Scharff-Schiott (LSS) theory.[9] As pointed out by Borders and Poate[10] and Cohen *et al.*,[11] this is likely due to the "feeding-in" effect: some of the Au atoms become channeled over part of their path, thus suffering lower energy loss than those traversing the crystal in random directions.

For lattice-location measurements using ion channeling the substitutional fraction of implanted atoms is defined as[12]

$$S=(1-\chi^i_{\min})/(1-\chi^h_{\min}) , \quad (1)$$

where $\chi^i_{\min}$ and $\chi^h_{\min}$ are the minimum yields for impurity and host, respectively.

More details on the lattice-site location can be obtained by comparing the normalized angular dependence of the scattering yield at a given depth for both host and impurity.

As shown in Fig. 2 for an as-implanted sample, the impurity and host scan curves match exactly, thus indicating the complete substitutionality of Au. It should be pointed out, however, that the 100% substitutionality of Au was obtained only for the crystals implanted with current densities less than 1 μA/cm^2. Higher current densities produced a significant decrease of the substitutional fraction. With regard to the annealing behavior of the Au-implanted Fe, which will be discussed in detail in the following section, we conclude that this is most probably due to beam heating during implantation. Thus the lattice occupation of Au occurs during the slowing-down process in the collision cascade and not by radiation-enhanced or thermally activated diffusion, which would lead to precipitation.

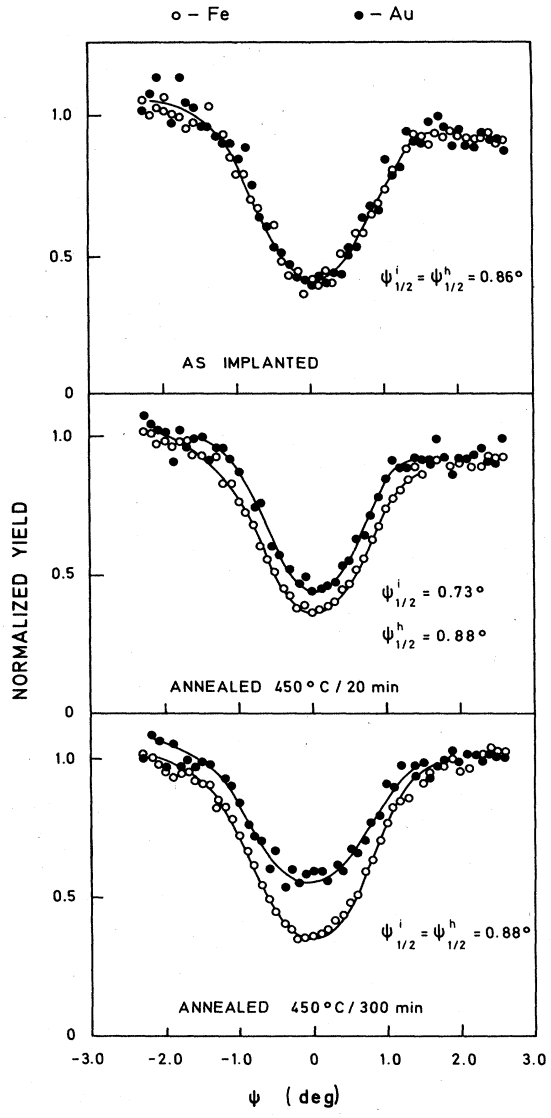

FIG. 2. Angular scans through the ⟨111⟩ axial direction.

B. Low-temperature annealing stage (300—500 °C)

The Au profile as shown in Fig. 1 does not change during thermal annealing in this temperature range. The most important changes are a narrowing of the angular scan curve for Au and an increase of the yield of the impurity peak in the aligned spectrum, indicating a loss of Au substitutionality. These results are demonstrated in Fig. 2, where angular scan curves are shown as measured through the ⟨111⟩ direction for the cases of isothermal annealing at 450 °C. After annealing at 450 °C for 20 min, the minimum yield for the impurity increased slightly. The narrowing of the angular scan curve by about 0.15° indicates that Au is displaced about 0.02 nm from the regular lattice sites. After prolonged (300 min) annealing at that temperature an equilibrium state is attained, which results in the reduction of the Au substitutional fraction. One notes that after the formation of noncoherent Au

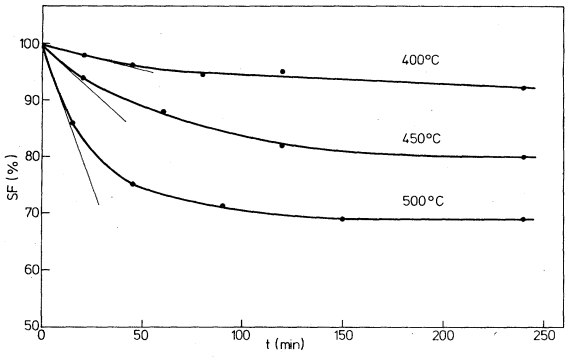

FIG. 3. Substitutional fraction of Au as a function of the anneal time at different annealing temperatures.

precipitates the critical angle for the substitutional fraction of the impurity is again equal to that of the host.

Figure 3 shows the kinetics of precipitation by measuring the substitutional fraction of Au obtained after annealing for different times t, at a given temperature T. Details will be discussed in Sec. IV B.

C. Intermediate-temperature annealing stage (550–650 °C)

Large changes in the Au depth distribution were observed after annealing at temperatures ranging from 550 to 650 °C. An example is given in Fig. 4, where the Au peak is shown before and after isothermal annealing at 600 °C. The heat treatment caused rapid precipitation of Au, accompanied by diffusion of the impurity towards the surface. As annealing progressed the surface peak increased at the expense of the as-implanted peak. There is no substitutionality of Au in the surface region. After annealing at 600 °C for about 100 min, a steady state is reached where neither the surface peak nor the substitutional fraction in the vicinity of the as-implanted peak changes any longer. In order to attain the complete dissolution of the as-implanted peak, a higher annealing temperature is necessary. Figure 5 shows the evolution of Au backscattering spectra for isothermal annealing at 650 °C. Here again the steady state is reached after prolonged heat treatment: the as-implanted peak disappeared, and the surface agglomeration of impurities has attained its maximum. Moreover, a tail of Au extending into the bulk is clearly visible, with all Au atoms in the tail occupying substitutional positions.

For a quantitative analysis the total amount of implanted atoms N_t was estimated from the Au peak area for as-implanted samples in the conventional manner.[8] Separately, the number of atoms N_s and N_M corresponding to the surface peak area and to the as-implanted peak area, respectively, were determined from the spectra. The time dependence of the N_s/N_t ratio, where N_t is equal to N_s+N_M, for isothermal annealing at 550, 600, and 650 °C, is shown in Fig. 6. The steady state was attained, where the ratio N_s/N_t was 0.28, 0.38, and 0.6 for 550, 600, and 650 °C, respectively. For the lower annealing temperatures the sum of N_s+N_M remained constant and

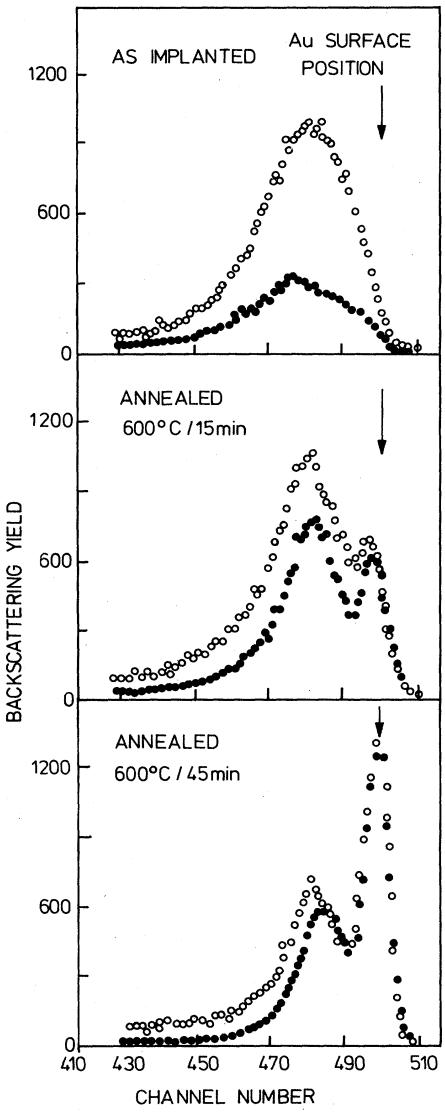

FIG. 4. Random and aligned backscattering spectra of the Au peak after isothermal annealing at 600 °C.

was equal to N_t. A somewhat different behavior was observed at 650 °C. Here again the surface peak grew initially at the expense of the as-implanted peak and the steady state was reached after annealing for 45 min. With prolonged annealing time the remainder of the as-implanted peak slowly disappeared, however, without any noticeable change of N_s. It is obvious that the transport of implanted atoms towards the surface is rapid as compared to the impurity loss by diffusion into the underlying bulk.

D. High-temperature annealing stage (above 650 °C)

Prolonged isothermal annealing at temperatures above 650 °C resulted in a reduction and a complete disappearance of the Au surface peak. The width of the peak is not affected in this stage of diffusion. A diffusion profile of Au extending to greater depth was observed with a concentration level remaining constant with the annealing

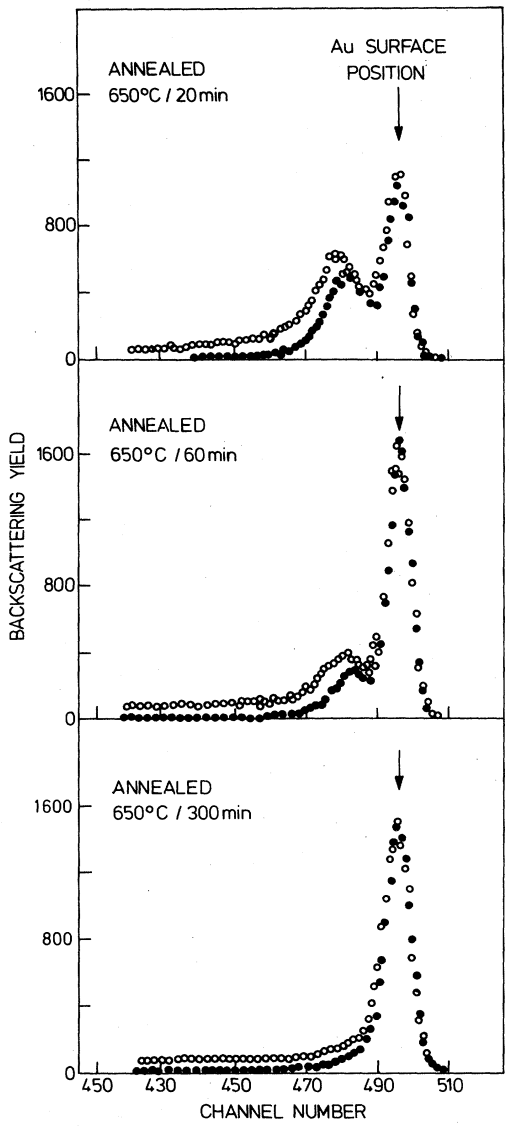

FIG. 5. Random and aligned backscattering spectra of the Au peak after isothermal annealing at 650 °C.

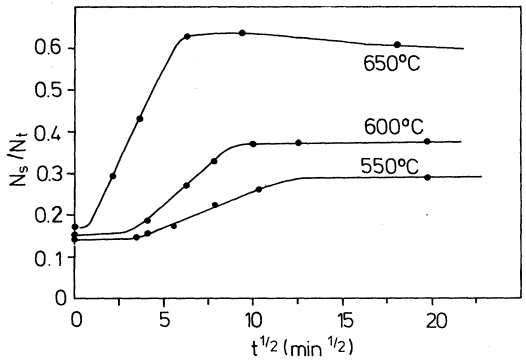

FIG. 6. Time dependence of the relative amount of Au which has diffused from the implanted region to form the surface agglomerate.

time. Only after the disappearance of the surface peak did the height of the diffusion tail decrease. Details will be discussed in Sec. IV D.

IV. INTERPRETATION OF EXPERIMENTAL RESULTS

A. Radiation damage in Fe

The annealing behavior of irradiated metals is governed by more or less distinct recovery stages which appear at temperatures where different defects become mobile,[13,14] as will be shortly summarized below for Fe. The defect mobility leads to their annihilation or clustering. They can also be captured by solute atoms.

The first recovery stage is attributed to the recombination of close Frenkel pairs and interstitial atom migration. At the end of stage I the large agglomerates of trapped interstitials as well as single and multiple vacancies are present. During stage II, detrapping of interstitials from larger complexes and subsequent annihilation at vacancies takes place. For Fe both stages set in below 200 K. The characteristic feature of stage III is the free migration of vacancies. Electrical-resistivity,[15] muon-spin-rotation,[16] and positron-lifetime[17] measurements have shown that this recovery stage is located in the temperature range above 200 K. In stage III the vacancies either annihilate at fixed sinks or form large immobile clusters which eventually anneal out in a further discrete stage located at a higher temperature. Electron-microscopy experiments[18,19] revealed that the vacancy clusters are mostly vacancy loops, preferentially located in {100} planes. At a higher temperature various rearrangement and coarsening processes occur (stage IV) until finally in stage V, at a temperature exceeding 750 K,[15] vacancy clusters anneal out, thus providing a large number of free vacancies.

The presence of impurities can influence the above-outlined scheme because of possible defect trapping. A series of channeling[20] and muon-spin-rotation[21] measurements have shown that the presence of Au in Fe leads, above the vacancy-mobility threshold, to vacancy—Au-atom pair formation. Upon annealing, vacancy clusters grow by agglomeration of vacancy-Au pairs and at the expense of smaller clusters.

After room-temperature implantation the highly mobile interstitials have annealed out and play no further role in damage evolution. The main feature of the defect pattern is the presence of vacancy-impurity clusters, vacancy loops, and a small number of isolated vacancies. Upon annealing, the damage evolution begins in stage IV and follows the above-outlined scheme.

B. Low-temperature annealing stage (350—450 °C)

The Fe samples were implanted with Au, producing a peak concentration of the impurity exceeding the solubility limit by a factor of more than 20. The degree of supersaturation is the main driving force for impurity precipitation. However, the excess of vacancies produced during ion implantation causes the precipitation to appear at lower temperatures than would occur under heat treatment alone.[22]

The lattice strain produced by the massive incorporation of the oversized Au atoms also influences the interaction between impurity atoms and lattice defects. The view that vacancies are necessary for nucleation of incoherent precipitates in order to relieve the volume stress is, in principle, widely accepted.[23] As discussed in the preceding section, at temperatures above stage III the vacancies form vacancy clusters or are trapped by Au atoms. However, since the channeling measurements for as-implanted samples have not shown any displacements of Au atoms from the lattice sites (cf. Fig. 2), we conclude that, if at all, only trapping of single vacancies or perhaps divacancies occur. The displacement of the solute in this case may be small ($\lesssim 0.01$ nm),[20] and thus cannot be detected by ion channeling. During annealing the single-vacancy Au atom pairs can migrate to form coherent precipitates, giving large solute displacement, as seen in Fig. 2 (450 °C, 20 min). Owing to the reduction of the nucleation barrier by vacancies,[23] incoherent Au precipitates form after prolonged annealing time. The decrease of the substitutional fraction of Au is then limited by the migration energy of complexes, which can be estimated as follows.

Assuming that vacancy-impurity pair migration can be described as a first-order kinetics, the concentration of such complexes can be calculated from

$$\frac{dc_{\mathrm{vi}}}{dt} = -p_t c_t c_{\mathrm{vi}} , \tag{2}$$

where c_{vs} is the concentration of vacancy-impurity complexes, c_t is the total trap concentration (including complexes themselves), and p_t is the probability of the complex-trap interaction, given by

$$p_t = \xi \nu \exp(-E_M/k_B T) , \tag{3}$$

where ξ is the geometrical factor,[24] ν is the jump frequency, and E_M is the migration energy of complexes.
Hence,

$$c_{\mathrm{vi}} = c_{\mathrm{vi}}^0 \exp(-p_t c_t t) . \tag{4}$$

The migration energy E_M can be calculated from the slope of the curves shown in Fig. 3 at $t=0$ using Eqs. (3) and (4), and it amounts to 1.0 eV. The structure of vacancy-impurity clusters and impurity precipitates have not yet been determined.

C. Intermediate-temperature annealing stage (550–650 °C)

When the annealing temperature is such that the thermal energy is higher than the sum of the vacancy migration energy and the binding energy of a vacancy in a vacancy cluster, the clusters begin to dissolve, thus providing an important source of mobile vacancies. A gradient of vacancy concentration implies a flow of defects with an accompanying transport of atoms.[24] Solute atoms may either flow against a vacancy flow (inverse Kirkendall effect) or, if they form mobile vacancy-impurity complexes, diffuse down their own concentration gradients. The complexes flow towards sinks and break up there, depositing the solute. Thus, the spatial redistribution of impurities is determined by the location of both sources and sinks for vacancies. At shallow depths the external surface is the dominant sink, and the atomic migration occurs essentially in one dimension.

For a quantitative interpretation of the kinetics of Au-surface segregation, we have applied the diffusion model of Lam, Okamoto, and Johnson[25] and Okamoto, Rehn, and Averback[26] developed for the analysis of radiation-induced segregation in alloys. The model is based on the assumption that the subsurface region of the sample is quickly drained of solute by the rapid diffusion of impurity complexes. Thus, the growth of the surface agglomerate is controlled by the transport of complexes across the depleted region. If the redistribution of the impurities does occur by diffusion of complexes, the binding energy of the vacancy-impurity pair must be sufficiently large and its migration energy sufficiently low that the complex will not dissociate during the time interval needed to reach the surface. Owing to stability arguments the impurity atom in the impurity-vacancy complex must occupy a substitutional position, i.e., only a small part of Au atoms, limited by the solid solubility at a given temperature, can form mobile complexes. The other part of the Au atoms which remains in the precipitates can be considered as a source maintaining the constant substitutional concentration of impurity atoms beneath the depleted zone.

The impurity flux through the depleted zone is given by

$$J_{\mathrm{vi}} = -D_{\mathrm{vi}} \frac{dc_{\mathrm{vi}}}{dx} , \tag{5}$$

where D_{vi} is the diffusion coefficient of vacancy-impurity complexes.

Since the atoms which agglomerate at the surface in a layer with thickness x_s come from the depleted region with a thickness x_d, conservation of the impurity concentration requires that

$$(c_s - c_0)x_s = c_0 x_d . \tag{6}$$

c_s and c_0 are the concentrations of Au atoms in the surface agglomerate and complexes in the bulk, respectively.

Assuming that the gradient in the concentration of complexes in the depleted region can be approximated by

$$\frac{dc_{\mathrm{vi}}}{dx} = \frac{c_{\mathrm{vi}}}{x_d} , \tag{7}$$

and combining Eqs. (5)–(7), one obtains, after integration,

$$x_s(t) = \left[\frac{2c_0 D_{\mathrm{vi}} c_{\mathrm{vi}}}{c_s(c_s - c_0)} (t - t_0) \right]^{1/2} . \tag{8}$$

To obtain the number of Au atoms in the surface agglomerate, $N_s(t)$, we assume that

$$c_{\mathrm{vi}} = K c_0$$

where $K \lesssim 1$, and $c_s \gg c_0$. Under these conditions Eq. (8) yields

$$x_s(t) = (K c_0/c_s)[2D_{\mathrm{vi}}(t - t_0)]^{1/2} . \tag{9}$$

Since

$$N_s(t) = x_s(t) c_s .$$

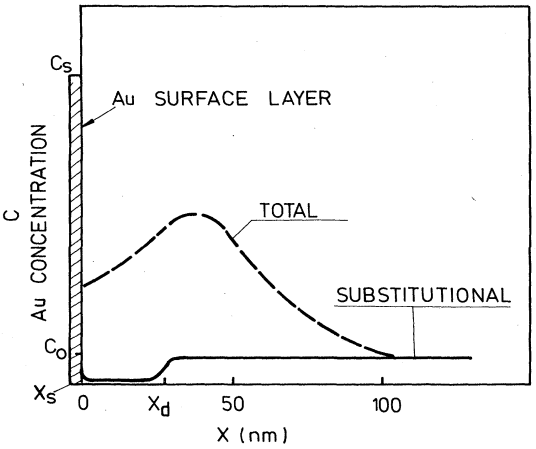

FIG. 7. Depth distribution of Au after annealing at 600 °C for 45 min.

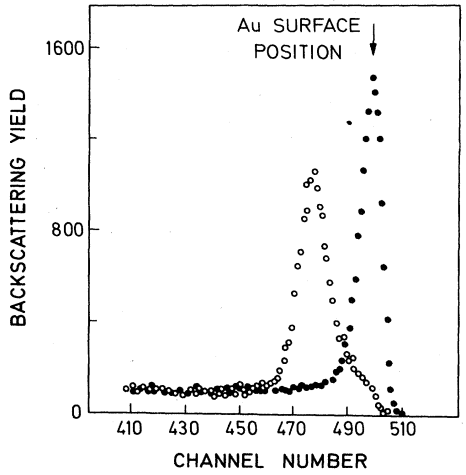

FIG. 8. Backscattering spectra obtained for a Au-implanted Fe single crystal with (○) and without (●) post-implantation with 5×10^{16} Ar^+ ions/cm^2 at 160 keV. The samples were annealed at 700 °C for 20 min.

one finally obtains

$$N_s(t)=K_1 c_0[D_{vi}(t-t_0)]^{1/2}, \tag{10}$$

where $K_1=\sqrt{2K}$.

Equation (10) shows that a certain time t_0 is required until the conditions are established under which the first Au atoms begin to agglomerate at the surface. One condition is that vacancies from the bulk reach the vacancy-depleted near-surface region so that Au-vacancy complexes will be formed there.

In light of the above discussion some features of the spectra shown in Figs. 4 and 5 should be pointed out. Firstly, the substitutional concentration (i.e., the difference between the yield of random and aligned spectra) in the depth interval corresponding to channel numbers 480—490 decreases with the annealing time at 600 °C. This indicates the formation of the depleted subsurface region. The depth distribution of Au after annealing at 600 °C for 45 min is shown schematically in Fig. 7. A similar depleted zone was produced after annealing at 650 °C for 20 min.

After prolonged annealing (cf. Fig. 6) the surface peak stops growing further, and at the same time the Au substitutional concentration in the subsurface region increases. This subsurface depletion is therefore a transient effect which persists as long as the flow of complexes does. Once the vacancy clusters anneal out, the subsurface region will not be drained any longer from the solute, and the equilibrium solubility concentration is reached. As can be seen from Fig. 6, the $t^{1/2}$ dependence of the surface-layer growth after some time t_0, as predicted by Eq. (10), is remarkably well reproduced by the experiment. In order to calculate the activation energy of the Au-vacancy—complex migration, the value of the solid solubility c_0 at the given temperature is needed. This can be determined from the backscattering yield difference of the aligned and random spectra (cf. Figs. 4 and 5). The c_0 values are listed in Table I. The calculated activation energy, 1.1 eV, is very close to the value of 1.0 eV obtained for the low-temperature annealing stage.

The time dependence of the surface agglomerate growth exhibits the saturation in $N_s(t)$ at values which are smaller than the total number of implanted atoms, N_t. The saturation level increases as a function of the annealing temperature. In principle, such a behavior is to be expected since the binding energy of vacancies increases with vacancy-cluster size.[27] Consequently, the small clusters anneal out at lower temperature, whereas for the release of vacancies from the large ones the evaluated temperature is necessary. Therefore, the number of free vacancies increases as a function of annealing temperature, producing larger flow of Au atoms.

In order to test the influence of spatial distribution and the strength of different sinks, an attempt has been made to produce an internal sink able to compete with the surface. Since the effectiveness of the surface sink for defects and, consequently, impurities, decreases with increasing depth, an additional sink has been formed at a depth of about 70 nm beneath the surface, i.e., corresponding to the maximum of the Au distribution. This was accomplished by post-implanting a Au-implanted Fe single crystal using 5×10^{16} Ar^+/cm^2 at 160 keV. Figure 8 shows a set of backscattering spectra obtained for samples with and without post-implantation. In contrast to the sample implanted only with Au, the surface peak does

TABLE I. Gold concentration c_0 just beneath the surface after rapid cooling from various temperatures.

T (°C)	550	600	650	680	730
c_0 (at. %)	0.15	0.20	0.35	0.46	0.67

not appear in the spectrum for the post-implanted sample. However, a sharpening of th Au profile is observed. It is known that implanted noble gases form bubbles by filling vacancy clusters. As these bubbles are rather stable, there are only a few additional vacancies available for Au precipitation and migration towards sinks at temperatures below 700 °C. This result supports the assumption that vacancy clusters formed during implantation in Fe at room temperature are the source of vacancies for the observed enhanced diffusion and segregation processes.

D. High-temperature annealing stage (over 650 °C)

Annealing at temperatures above 650 °C causes a reduction in the amount of Au at the surface, but the concentration of the diffused tail remains constant as long as the gold agglomerate exists. Since Au has a vapor pressure of $\sim 10^{-9}$ Torr at 750 °C, the loss of Au by evaporation at the surface is negligible.

It is worth noting that the concentration in the tail at a given depth depends only on the annealing temperature and is independent of anneal time and the magnitude of the surface agglomerate. When Au diffuses from the surface agglomerate, it is 100% substitutional, indicating that it moves by the vacancy mechanism. Therefore, the behavior of the diffused tail reflects the solid solubility of Au in Fe. As shown by Myers and Smugeresky,[28] in such a case the concentration of the diffused tail where it intersects the surface peak is a measure of the solid solubility. The Au concentration just beneath the surface was calculated from the backscattering spectra and is listed in Table I.

Moreover, the amount of Au atoms per unit area $Q(t)$ which has diffused from the surface agglomerate should vary with isothermal annealing time as $t^{1/2}$.[29] The total amount of atoms which are left in the surface agglomerate, $N_1(t)$, is given by

$$N_1(t)=N_s^0-Q(t)\ , \tag{11}$$

where N_s^0 is the initial number of atoms in the surface agglomerate. The variation of N_1/N_s^0 with $t^{1/2}$ for a series of isothermal annealing runs is shown in Fig. 9. As can be seen in Fig. 9, the square-root dependence is not completely confirmed. Consequently, analysis of the data requires a more refined model for the evolution of the Au depth distribution. The complicating factor is that a preliminary annealing step is necessary in order to produce the surface agglomerate. During this step the Au atoms migrate not only towards the surface but also diffuse into the bulk. Moreover, the spectra in Figs. 4 and 5 indicate that at the depth corresponding to the implanted layer some of the Au atoms always occupy substitutional positions. The concentration of these atoms is limited by the solid solubility at a given temperature.

The analytical model to be presented here applies the diffusion equation to the entire Au-Fe system with the initial distribution of Au as shown in the inset of Fig. 9.

The diffusion equation has been solved for the boundary conditions

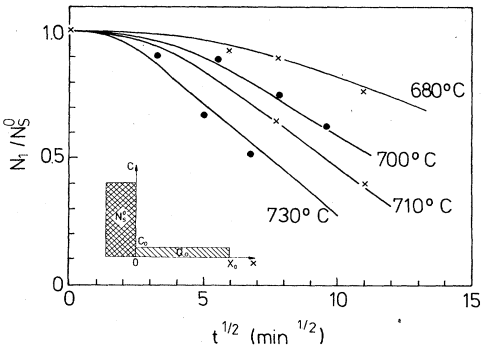

FIG. 9. Time dependence of the relative amount of Au in the surface agglomerate. The inset shows the initial depth distribution of Au as used for diffusion calculations by means of Eq. (14).

$$c(0,t)=c_0\ ,$$

$$c(x,0)=\begin{cases} c_0, & 0\le x\le x_0 \\ 0, & x>x_0 \end{cases}$$

using the method developed for the diffusion from a constant source,[29] yielding the solution

$$c(x,t)=c_0\left\{1-\frac{1}{2}\left[\operatorname{erf}\left[\frac{x_0+x}{2\sqrt{Dt}}\right]-\operatorname{erf}\left[\frac{x_0-x}{2\sqrt{Dt}}\right]\right]\right\}. \tag{12}$$

The net flow of atoms per unit area from the source is given by

$$J(t)=-D\left.\frac{\partial c}{\partial x}\right|_{x=0}=\frac{Dc_0}{\sqrt{\pi Dt}}e^{-x_0/2\sqrt{Dt}}\ . \tag{13}$$

The amount of atoms which have diffused from the surface agglomerate is determined by

$$Q(t)=\int_0^t J(\tau)d\tau$$

$$=\frac{c_0x_0}{\sqrt{\pi}}\left[\frac{2\sqrt{Dt}}{x_0}e^{-x_0/2\sqrt{Dt}}-E_1\left[\frac{x_0}{2\sqrt{Dt}}\right]\right], \tag{14}$$

where $E_1(x_0/2\sqrt{Dt})$ is the integral exponential function.

In devising experimental tests for the validity of the above model, we note that the experimentally accessible parameters are N_t, N_s^0, and c_0. Equation (11) was solved for initial values characteristic of the present experiments:

$$N_t=Q_0+N_s^0=5\times 10^{16}\ \text{atoms/cm}^2\ ,$$

with $Q_0=c_0x_0$ and $Q_0/N_s^0=0.4$. The typical value for x_0 amounts to 400 nm.

In analyzing the experimental data to obtain the diffusion coefficient, the time dependence of the area under the Au surface peak is calculated according to Eq. (11). This calculated function is compared with the experimentally measured kinetics shown in Fig. 9, and the diffusion coefficient D is adjusted to produce the best agreement. The fit yields the preexponential factor $D_0\cong 100\ \text{cm}^2/\text{sec}$ and the activation energy $E_a=2.9$ eV. The present dif-

fusion results are believed to reflect bulk diffusion, substantially unaffected by the lattice damage. Once the surface agglomerate is formed, the channeling minimum yield $\chi^h_{\min}$ is close to that of the unimplanted Fe single crystal,[7] thus indicating the absence of defects.

While the surface agglomerate does not show any channeling pattern for both ⟨111⟩ and ⟨100⟩ orientations of the host crystal, a $\chi^i_{\min}$ value of 80% was measured for the ⟨110⟩ direction. We attribute this to the texture of the polycrystalline Au surface agglomerate induced by its partially epitaxial growth. The interatomic spacing of the host Fe atom in the ⟨110⟩ direction is 4.055 Å; that of Au along the ⟨100⟩ is 4.078 Å. However, no influence of this texture effect of the Au back-diffusion was noticed.

V. SUMMARY AND CONCLUSIONS

Annealing studies have been made on Au-implanted Fe single crystals. The doses chosen were such that the solid solubility of Au in Fe is greatly exceeded. We have shown that the various temperature dependences of the impurity segregation are strongly influenced by the annealing of defect agglomerates. The observed solute redistributions occur via a three-step mechanism. At relatively low (350—500 °C) temperatures a short-range migration of vacancy-impurity complexes causes Au precipitation. In the intermediate-temperature range (550—650 °C) the migration of vacancy—Au-atom clusters produces a rapid transport of the impurity to the surface and its segregation there. The Au surface layer is observed to grow epitaxially on a Fe(110) surface. After further increase of the annealing temperature above 650 °C, Au diffuses backwards from the surface by the vacancy mechanism and is substitutional in Fe.

The experimental results indicate that three factors are primarily responsible for the temperature dependence of Au distribution:

(1) The freely migrating vacancy concentration which is first reduced due to clustering reaches a maximum when the clusters decay, and finally attains an equilibrium concentration after the surplus vacancies have annihilated at sinks. The surface is normally the strongest sink. However, after post-implantation with Ar ions a competing sink can be produced consisting of vacancy clusters filled with Ar atoms.

(2) The degree of coupling between impurity and vacancies varies with temperature. At intermediate temperatures, where it is maximal, significant impurity participation in the defect flux does occur.

(3) The back-diffusion of Au is determined by bulk diffusion in the state of thermodynamic equilibrium.

This kind of annealing behavior has also been observed for other implants of Pt and Pb in Fe,[30] and we anticipate that a behavior such as that observed in this experiment will occur frequently for metal-in-metal implanted systems produced by implanting oversized ions.

ACKNOWLEDGMENTS

We would like to thank J. Geerk, G. Linker, and A. Skorupski for helpful discussions.

*Permanent address: Institute for Nuclear Studies, Warsaw, Poland.

[1]S. M. Myers, in *Proceedings of the International Conference on Ion Beam Modifications of Materials,* edited by J. Gyulai, T. Lohner, and E. Pasztor (Central Research Institute for Physics, Budapest, 1978).

[2]J. M. Poate and A. G. Cullis, in *Ion Implantation, Treatise on Materials Science and Technology,* edited by J. K. Hirvonen (Academic, New York, 1980).

[3]A. R. Miedema, Philips Tech. Rev. **36**, 217 (1976).

[4]*Metastable Materials Formation by Ion Implantation,* edited by S. T. Picraux and W. J. Choyke (Elsevier, New York, 1982).

[5]*Phase Transformations During Irradiation,* edited by F. V. Nolfi (Applied Science, New York, 1982).

[6]H. Ferber, H. Kasten, G. Wolf, W. Lorenz, H. Schweckert, and H. Folger, Corros. Sci. **20**, 117 (1980).

[7]A. Turos, H. Alberts, and O. Meyer, Nucl. Instr. Methods **209—210**, 1041 (183).

[8]W. K. Chu, J. W. Mayer, and M.-A. Nicolet, *Backscattering Spectrometry* (Academic, New York, 1978).

[9]J. Lindhard, M. Scharff, and H. Schiøtt, Kgl. Dansk. Vidensk. Selsk. Mat.-Fys. Medd. **33**, 14 (1963).

[10]J. A. Borders and J. M. Poate, Phys. Rev. B **13**, 969 (1976).

[11]C. Cohen, F. Abel, M. Bruneaux, L. Thomé, H. Bernas, and J. Chaumont, Phys. Rev. B **20**, 1780 (1979).

[12]S. T. Picraux, in *New Uses in Ion Accelerators,* edited by J. F. Ziegler (Plenum, New York, 1975).

[13]W. Schilling, G. Burger, K. Isebeck, and H. Wenzl, in *Vacancies and Interstitials in Metals,* edited by A. Seeger, D. Schuhmacher, W. Schilling, and J. Diehl (North-Holland, Amsterdam, 1970).

[14]R. W. Balluffi, J. Nucl. Mater. **69—79**, 240 (1978).

[15]W. Glaeser and H. Wever, Phys. Status Solidi **35**, 367 (1969).

[16]A. Möslang, H. Graf, E. Recknagel, A. Weidinger, Th. Wickert, and R. I. Grynszpan, in *Point Defects and Defect Interactions in Metals,* edited by J. Takamura, M. Doyama, and M. Kiritani (University of Tokyo Press, Tokyo, 1982).

[17]P. Hautojärvi and A. Vehanen, Radiat. Eff. Lett. **58**, 77 (1981).

[18]N. Yoshida, M. Kiritani, and F. E. Fujita, J. Phys. Soc. Jpn. **39**, 170 (1975).

[19]M. L. Jenkins, C. A. English, and B. L. Eyre, Philos. Mag. A **38**, 97 (1978).

[20]M. L. Swanson and L. M. Howe, Nucl. Instrum. Methods **218**, 613 (1983).

[21]A. Weidiger, quoted in Ref. 20.

[22]P. Wilkes, J. Nucl. Mater. **83**, 166 (1979).

[23]K. C. Russell, Scr. Metall. **3**, 313 (1969).

[24]R. A. Johnson and N. Q. Lam, Phys. Rev. B **13**, 4364 (1976).

[25]N. Q. Lam, P. R. Okamoto, and R. A. Johnson, J. Nucl. Mater. **78**, 408 (1978).

[26]P. R. Okamoto, L. E. Rehn, and R. S. Averback, J. Nucl.

Mater. **108—109**, 319 (1982).
[27]A. Signer and D. Kuhlman-Wilsdorf, Phys. Status Solidi **21**, 545 (1967).
[28]S. M. Myers and J. E. Smugeresky, Metall. Trans. **8A**, 609 (1977).
[29]B. I. Boltaks, *Diffusion in Semiconductors* (Infosearch, London, 1963).
[30]A. Turos and O. Meyer, Mater. Sci. Eng. **69**, 49 (1984).